Applied Thermal Engineering 279 (2025) 127656

Contents lists available at ScienceDirect

Applied Thermal Engineering

journal homepage: www.elsevier.com/locate/apthermeng

Research Paper

Porosity effect of bio-coated surfaces on flow boiling heat transfer of HFE-7000☆

Mandana Mohammadilooey [a,b,c], Zülal Muganlı [a,b], Soroush Niazi [a,b,d], Gül Kozalak [a,f], Erçil Toyran [a,b], Hyun Sun Park [e], Ali Sadaghiani [a,b,f,g], Ali Koşar [a,b,f,*]

[a] Faculty of Engineering and Natural Sciences (FENS), Sabanci University, Orhanli, 34956 Tuzla, Istanbul, Turkey
[b] Sabanci University Nanotechnology and Application Center (SUNUM), Sabanci University, Orhanli, 34956 Tuzla, Istanbul, Turkey
[c] Department of Mechanical Engineering, The Pennsylvania State University, University Park, PA 16802, USA
[d] Department of Mechanical and Aerospace Engineering, University of Central Florida, 32816 Orlando, FL, USA
[e] Department of Nuclear Engineering, Nuclear Research Institute for Future Technology and Policy, Seoul National University, Seoul, Republic of Korea
[f] Center of Excellence for Functional Surfaces and Interfaces for Nano-Diagnostics (EFSUN), Sabanci University, Orhanli, 34956 Tuzla, Istanbul, Turkey
[g] Department of Mechanical Engineering, School of Engineering, University of Birmingham, Birmingham B15 2TT, UK

ARTICLE INFO

Keywords:
Bio-coating
Microporosity
Saccharolobus solfataricus
Flow boiling
Heat transfer enhancement
HFE-7000

ABSTRACT

Surface modification has emerged as a prominent approach for providing ultra-high heat flux cooling and enhancing boiling heat transfer of particularly dielectric fluids, where inherent limitations such as low thermal conductivity and latent heat deteriorate the performance. Despite the large number of methodologies in surface modification for enhanced boiling heat transfer, a considerable proportion of surface modification techniques necessitate access to cleanroom facilities or involve protracted procedures, including the utilization of environmentally hazardous materials. This study presents flow boiling heat transfer results of HFE-7000 in a rectangular high aspect ratio minichannel with a coated surface using proposed environmentally friendly and economical microbial bio-coating (*Saccharolobus solfataricus P2* bio-coatings). The boiling heat transfer characteristics of bio-coated surfaces, which were optimized in terms of coating structure and durability against the fluid flow by the dip mixed coating method, were explored. Flow boiling experiments were performed on coated surfaces at heat fluxes ranging from 5.4 to 50.9 W/cm^2, mass flux of 500 kg/m^{2}s, inlet subcooling of 10 °C, and atmospheric pressure. Bubble dynamics and flow boiling patterns were obtained using a high-speed camera. The bio-coated surface offered significant heat transfer enhancement compared to the bare silicon sample by offering more active nucleation sites and showing resistance to vapor film/dry spot formation on the surface by providing a porous structure. This porous architecture not only increases the density of nucleation sites but also enables capillary-driven rewetting, which sustains thin liquid films and delays dry-out at high heat fluxes. The coated surface achieved the highest heat transfer coefficient, with a maximum enhancement of 50 %, and enhanced the critical heat flux (by a factor of about 1.5 relative to the plain surface) by stabilizing two-phase flow and promoting rewetting.

1. Introduction

Thermal management systems prevent overheating at crucial locations such as hot spots and ensure safe operation of various systems and miniature devices. As a part of the 4th Industrial Revolution, the semiconductor industry continues expanding, with growing sales by more than 20 % in 2021, and has a huge impact on many sectors, including the automotive industry, artificial intelligence, and data storage [1]. Despite significant growth, cooling of miniature devices has remained an issue for the semiconductor industry, and high heat flux cooling as high as 1.5 kW/cm^2 has been sought [2]. Flow boiling heat transfer of dielectric liquids in mini- and microchannels has been employed due to its high potential in electronics cooling [3]. Dielectric fluids with low saturation temperature, less corrosivity, and adaptability to immersion cooling (direct contact cooling) can maintain the working temperature within a safe range [2]. Despite these advantages, poor thermophysical

☆ This article is part of a special issue entitled: 'Micro-FloTec' published in Applied Thermal Engineering.

* Corresponding author at: Faculty of Engineering and Natural Sciences (FENS), Sabanci University, Orhanli, 34956 Tuzla, Istanbul, Turkey.
E-mail address: kosara@sabanciuniv.edu (A. Koşar).

https://doi.org/10.1016/j.applthermaleng.2025.127656
Received 16 November 2024; Received in revised form 7 July 2025; Accepted 22 July 2025
Available online 23 July 2025

properties such as the latent heat of vaporization, liquid-specific heat, low surface tension, and high air solubility are some of the inherent issues related to dielectric fluids [2]. Fluorocarbon-based (Fluorinert) liquids have been generally used as dielectric elements in related studies [4–6]. In addition to its excellent dielectric properties, HFE-7000 with its non-flammability and non-corrosiveness, zero ozone depletion potential, very low global warming potential, and optimum operating temperature of 34.0 °C at atmospheric pressure, has become a strong candidate as a working fluid [7–10]. However, high wall temperature overshoot at the inception of saturated boiling, high-pressure drop associated with the vapor formation, and occurrence of flow instabilities might occur in flow boiling of highly wetting dielectric fluids [11]. Possible solutions to address these issues could be surface modification to have an earlier onset of nucleate boiling (ONB)[6], to mitigate boiling instabilities [11] and to raise critical heat flux (CHF) and heat transfer coefficient (HTC) [11,12].

In a typical flow boiling curve, single-phase natural convection from the heater initially occurs, followed by the formation of bubbles due to nucleate boiling. The onset of nucleate boiling (ONB) varies depending on the surface characteristics. As the temperature from the heater increases, more nucleation sites appear, and bubbles from the surface rise, leading to the formation of vapor columns on the surface. At a critical point, vapor columns cover the surface like a blanket and delay the cooling process. This phenomenon is associated with critical heat flux (CHF). Different surface modification methods have been implemented to enhance both boiling heat transfer and CHF. These methods include nanowire arrays [13], nanorods [14], graphene coating [15], polymer coating [16], virus coating [17], biphilic surfaces [18], laser-engineered surfaces [19] and plasma spray coating [20]. Additionally, altering the surface texture has been employed as a passive heat transfer enhancement technique to enhance the flow boiling heat transfer performance of dielectric fluids [21]. Micro-scale roughness and microporous structures are the approaches that have an impact on CHF and can be applied to the surface by additive and subtractive methods [10]. These techniques were proven to enhance boiling heat transfer by providing surface enhancement and artificial nucleation sites [22,23].

Surface microtextures are among the most studied techniques to enhance the heat transfer performance and improve nucleate boiling heat transfer by adjusting liquid–vapor interactions, increasing active nucleation site density, and assisting in liquid rewetting. Jiao et al. [25] demonstrated that hierarchical microstructured surfaces can enhance HTC by altering the surface wettability and vapor dissipation. Similarly, engineered structured surfaces with micro/nanotextures were shown to increase CHF by up to 80 % in high-heat flux applications [26]. However, the scalability and application of these techniques in large-scale cooling systems are limited due to their requirement for complex manufacturing processes such as photolithography or electrochemical etching.

One of the major limitations of nanoparticle-based coating methods is the channel blockage due to nanoparticle agglomeration [24]. Although metal coatings offer high thermal conductivity, which can improve heat transfer performance, weak adhesion of the metal-coated nanoparticles to the substrate leads to particle detachment and accumulation within the flow channel, which causes mechanical damage to the equipment in the loop during long-term operation.

In a previous study by White et al. [25], a significant portion of ZnO nanoparticles was observed to detach from the base substrate after pool boiling experiments of all samples, especially after the second experimental run. Although a significant enhancement in HTC compared to the base substrate was initially observed, the dislodged particles presented a concern in a flow boiling process, where shear lift and buoyancy forces can transport the particles, causing clogging in the channel [26]. Similar challenges have been recognized in other coating structures as well, including nanofibers, nanowires, nanotubes, nanoporous coatings, and nanofilms.

Another issue is chemical erosion, where metal oxide is formed due to the exposure of the coating metal particles to the oxygen content in the coolant. Lee et al. [27] reported a 37 % reduction in HTC after five repeated boiling tests using the aluminum-based porous coated surface. The deterioration was attributed to the reduction of the nucleation sites because of the formation of aluminium hydroxide within surface cavities.

In addition to the performance degradation, the high cost and harmful environmental effects associated with most of the surface modification techniques limit their large-scale applicability [28]. For instance, although laser texturing proposes high precision, it is not scalable for industrial applications due to the need for equipment maintenance and its substantial energy consumption. Similarly, electrochemical deposition and chemical etching processes involve environmentally hazardous waste materials, making them unsustainable for industrial applications [28]. Furthermore, some micro-texturing methods are constrained by the substrate material [28]. For example, the etchant should be compatible with the substrate in the wet etching process [29]. Mechanical surface modification methods, although cost-effective, can only be applied to hard materials and may damage softer materials. Additionally, they offer limited control over the surface geometry and the roughness profile [30].

The bio-inspired superhydrophobic coating is another method that has been investigated due to its potential to improve the effectiveness of vapor removal in boiling systems. According to Liu et al. [31], superhydrophobic coatings with hierarchical structures can delay dry-out conditions by promoting quick bubble departure. However, despite these advantages, superhydrophobic coatings frequently have wettability loss, heat deterioration, and durability limitations under extended boiling conditions [32], which limits their long-term efficiency.

In contrast to conventional methods, the bio-coating surface modification technique presents an environmentally compatible alternative. This method uses bio-compatible *Saccharolobus solfataricus P2* and biopolycations and a dip coating process to prepare porous and rough structures on metallic and non-metallic substrates [33,34]. Polyelectrolyte adsorption facilitates strong adhesion of the coating to the substrate and durability of the coating against flow, as oppositely charged polymer layers are electrostatically bonded to each other. It was demonstrated in previous studies by the authors [33,34] that bio-coated surfaces could preserve up to 92.9 % of the coating after two days of continuous water flow exposure.

Moreover, the employed dip coating process in this study consumes less energy compared to high-energy alternatives, e.g., laser texturing. Therefore, the coating approach in this study has an advantage in industrial scalability. Furthermore, this study proves that bio-coated surfaces not only perform effectively in the flow boiling of deionized water but also exhibit superior heat transfer performance when tested with dielectric fluids, which have lower thermophysical properties than water. An additional advantage of the bio-coating method is that different sizes and roughness geometries and porosity shapes that are difficult to achieve using conventional techniques are viable by modifying the process parameters, e.g., coating drying temperature [34].

This study aims to explore the application of Saccharolobus solfataricus P2 bio-coating as a novel and scalable surface modification method to improve flow boiling heat transfer in contrast to these traditional methods. This coating provides a special blend of improved wettability, increased nucleation site density, and long-term adhesion stability, in contrast to synthetic coatings. Additionally, the bio-coating preserves its hydrophilic properties and thermal stability during extended boiling conditions, in contrast to bio-inspired superhydrophobic coatings.

Archaeon cells are single-celled organisms without a nucleus and have a prokaryotic structure. They are like eukaryotic cells since they have circular chromosome and are capable of DNA replication and transcription [35]. *Saccharolobus solfataricus P2* is thermophilic archaea and stains gram-negative. It can be isolated from Pisciarelli Solfatara volcanic hot springs in Italy. In 2018, its nomenclature was changed and

transferred from the genus *Sulfolobus* to *Saccharolobus* [36]. Although they are considered as only sulfur-dependent extremophiles within the Thermoprotei class, they are separated from other archaea thanks to their rRNA sequences [37]. These archaeons have some features that enable them to withstand extreme physiological conditions. They can survive at temperatures ranging from −2 to 15 °C or 60 °C to 122 °C, salinity ranging from 2 to 5 °C, and conditions where pH is < 4 or > 9 [38]. *Saccharolobus solfataricus* has irregular lobes and flagellum [39]. It grows optimally between 80–85 °C temperature and pH 2 to 4 [39]. It is a good model thermophile that can be cultured under laboratory conditions with its aerobic respiration and chemoorganotrophic nutrition. Thanks to these features as well as its ability to remain attached to the surface even though it becomes dead, it has started to be used frequently in multidisciplinary studies, especially involving heat transfer research [34,40,41].

In this study, bio-coatings were prepared using *Saccharolobus solfataricus P2*, which is known for its resistance to extreme conditions. The preparation was made using the dip-coating method which could also be adapted to large-scale preparation to be implemented to commercial thermal-fluid systems. The effect of the coated surface structure on heat transfer and CHF enhancement in flow boiling of HFE-7000 was investigated for a rectangular minichannel. Flow patterns were visualized and linked to performance enhancement. The proposed bio-coating method is innovative, economical, scalable, and environmentally friendly, contributing to energy saving and environmental sustainability.

2. Experimental section

2.1. Sample preparation

Saccharolobus solfataricus P2 (35092) was obtained from the American Type Culture Collection (ATCC) and cultured with ATCC 1304 medium. The first inoculation was made with 30 ml of pre-warmed medium and for continued growth, 2 g/L D-sucrose was added to the medium. Archaea were incubated at 84 °C and pH 3.9. Cell proliferation was measured using UV Spectrophotometry at OD600, while gradually increasing the culture volume to 500 ml. When the absorbance of the archaeal culture reached 1.7, it was cooled on ice and centrifuged at 7000*g* for 10 min. 250 ml of culture was collected, and the remaining part was combined with 500 ml of fresh medium to ensure continuity of proliferation. For the experimental process, the supernatant was removed after centrifugation and stored at −80 °C. Preserved samples were first washed in 300 ml of phosphate buffer (20 % (v/v) in H_2O) at room temperature and then resuspended with 250 ml of fresh phosphate buffer to prepare for the bio-coating process (Fig. 1, Fig. 2). To increase the surface adhesion efficiency, Poly-L-Arginine (PLA) was added to the mixture at a ratio of 1:5 and applied to the 500 μm-thick silicon substrate. These coating parameters were selected according to the optimum solution in terms of the coating durability in the light of the results of the durability test in our previous study [34], where the durability was examined by comparing the thickness of the coating that was exposed to the water flow with a pumping speed of 1000 rpm for two days and the unexposed sample. The sample was dried at 60 °C for 1 h in the evaporator in the clean room. The detailed coating process was described in our previous studies [34,40].

Before characterization tests, surface fixation of *Saccharolobus solfataricus* cells on the silicon surface was conducted by glutaraldehyde solution. For this purpose, a solution of 4 % glutaraldehyde was utilized to treat bio-coated samples at room temperature for two hours. Following the fixation process, the bio-coated samples were washed with 0.1 M phosphate buffer saline (PBS). Subsequently, various concentrations of ethanol solutions including 30 %, 50 %, 70 %, 80 %, 90 %, 95 %, and 100 % were prepared, and dehydration of the bio-coated samples in intervals of 5 min each was performed. The surface morphology of the bio-coated silicon surfaces was characterized by scanning electron microscopy (SEM) (JEOL JSM 6010 W-SEM). Before the SEM analysis, the bio-coated surface was coated with a thin layer (4 nm) of gold–palladium alloy by using an SEM sputter (Nanovak NVTS 400 2 DC 1 RF Sputter System). After, microscale images of the bio-coated surfaces were taken at 45 °C titled visions. The contact angle (CA) measurements on the bio-coated/plain silicon surfaces were conducted to evaluate the surface wettability of the developed surfaces by CA device (Theta lite Contact Angle Measurement System). For this purpose, 5 μL of the water drop was applied to the center of the surfaces, and the CA measurements were determined. The thickness of the coating on the silicon surface was determined by a surface profilometer (KLA Tencor surface profiler).

2.2. Flow boiling experimental setup

Fig. 3 shows the schematic of a closed-loop flow boiling experimental setup. The setup allows pressure and temperature measurements and flow control inside the loop. A vane pump (1) (TCS Micropumps – V4000, UK) delivered the stored working fluid (HFE-7000) in a fluid container (2) at room temperature through the loop with a desired flow velocity. The mass flow rate was adjusted and measured by a metallic tube flowmeter (3) (Gentek – Metal Tube Flowmeter (1 % accuracy), Turkey). The fluid then passes through a preheater (4) (liquid-to-liquid heat exchanger) to maintain the desired level of subcooling at the inlet. The tubing between the preheater and test section was thermally insulated to reduce the heat losses. A particulate filter (5) was mounted prior to the inlet in order to prevent the contaminants from entering the test section. Two thermocouples (T-type – Omega) were located just before and after the test section and connected to a thermometer (6) to measure the inlet and outlet fluid temperatures. Wall temperatures were measured using 3 thermocouples located along the flow direction at 4 mm below the channel bottom surface. A Variac power supply (7) (GVN VRK VRK-M1) provided the desired input heat to the 6 cartridge heaters, each having a total electrical power input of up to 500 W, which were inserted into the holes inside the aluminum block. Digital pressure gauges (8) (MESENS-MPG100 (1 % accuracy)) before the inlet and after the outlet of the test section were used to measure the differential pressure. A high-speed camera (full–pixel resolution of 1920 × 1080 at a frame rate of 3000 fps) (9) that was connected to the computer (10) recorded the flow pattern during phase change through the transparent polycarbonate. The partially vaporized fluid at the outlet of the test

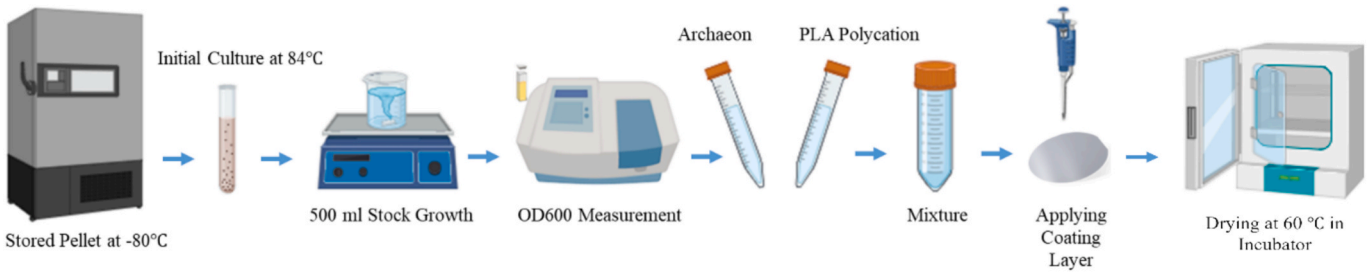

Fig. 1. The summary illustration of sample preparation and bio-coating process.

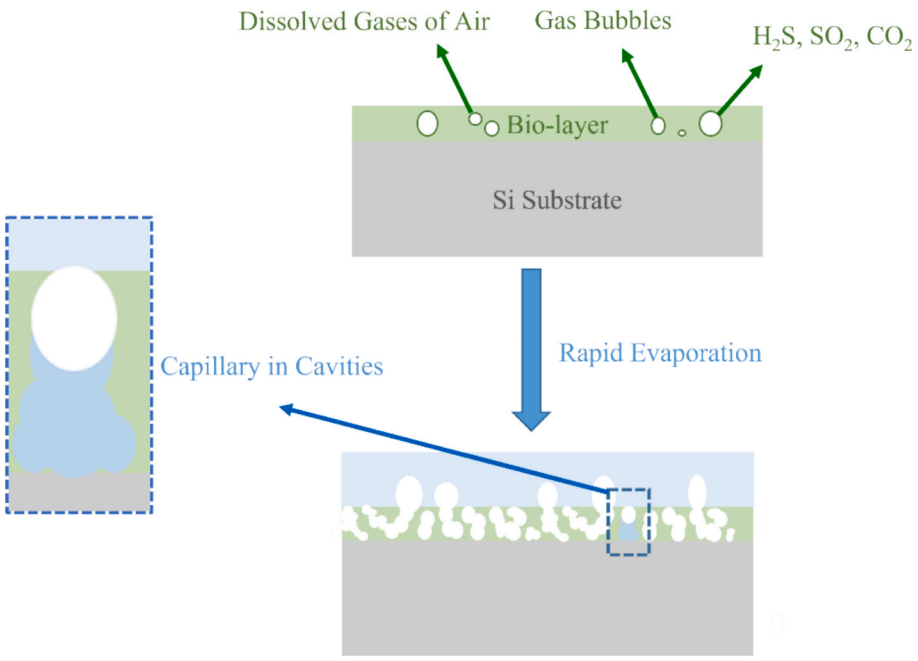

Fig. 2. The schematic illustration of porous structure formation after incubation at 60 °C.

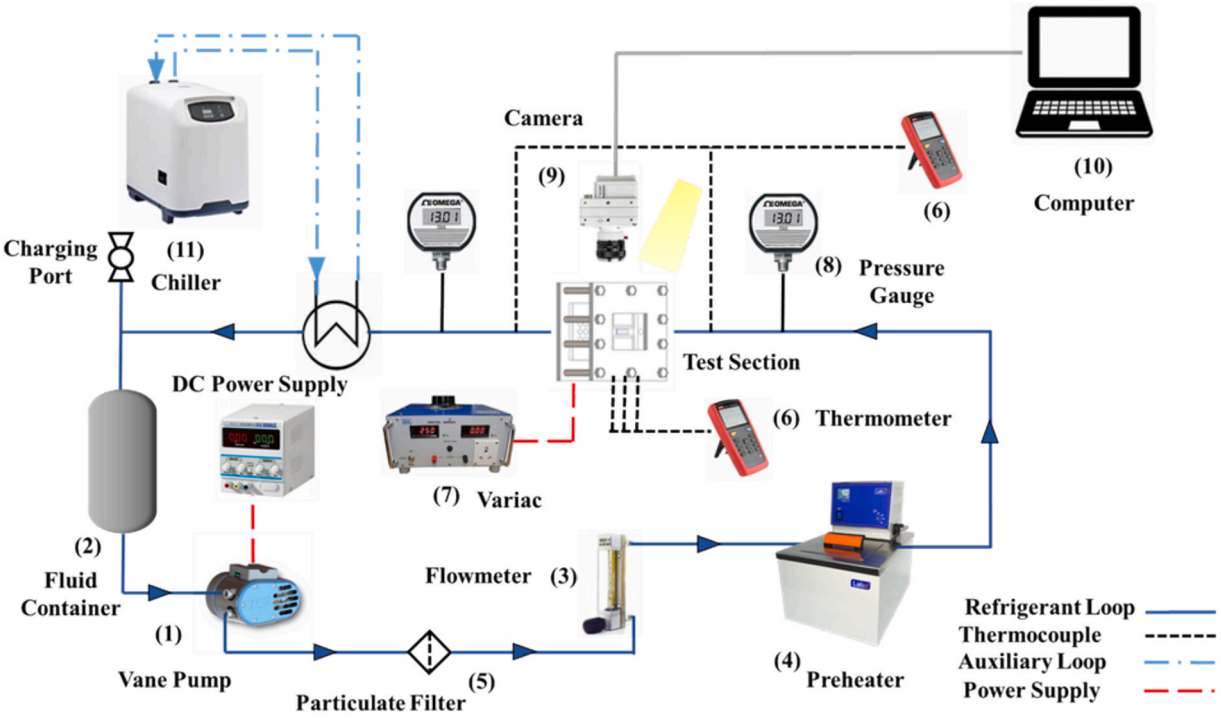

Fig. 3. Schematic of the closed-loop flow boiling experimental setup.

section was passed through an axillary condenser loop (11) (Counter flow heat exchanger and a chiller (Teco)) to be condensed and returned to the container. This cycle was repeated for each input of electrical power to generate boiling curves and calculate heat transfer coefficients.

Fig. 4 shows the expanded view of the test section. The test section includes top and bottom aluminum holders for fastening and sealing the test section, a main and bottom PTFE housing for insulation, a transparent polycarbonate plate for visualization, and an aluminum heating block for placement of cartridge heaters. The main Teflon housing consists of inlet and outlet plenums, thermocouple ports, and a machined groove to place the O-ring around the channel. The O-ring was pressed between the transparent top polycarbonate plate and grooved channel to ensure sealing. The transparent polycarbonate provides both visualization and thermal insulation. The silicon test pieces were placed on the top surface of the aluminum block. A superconductive thermal paste was used to minimize the thermal resistance between the sample and heating wall. Six holes were drilled through the length of the aluminum block to house cartridge heaters and to ensure that the supplied desired input power was uniformly distributed in the aluminum block across the 50 × 15 mm surface area. The gap between the

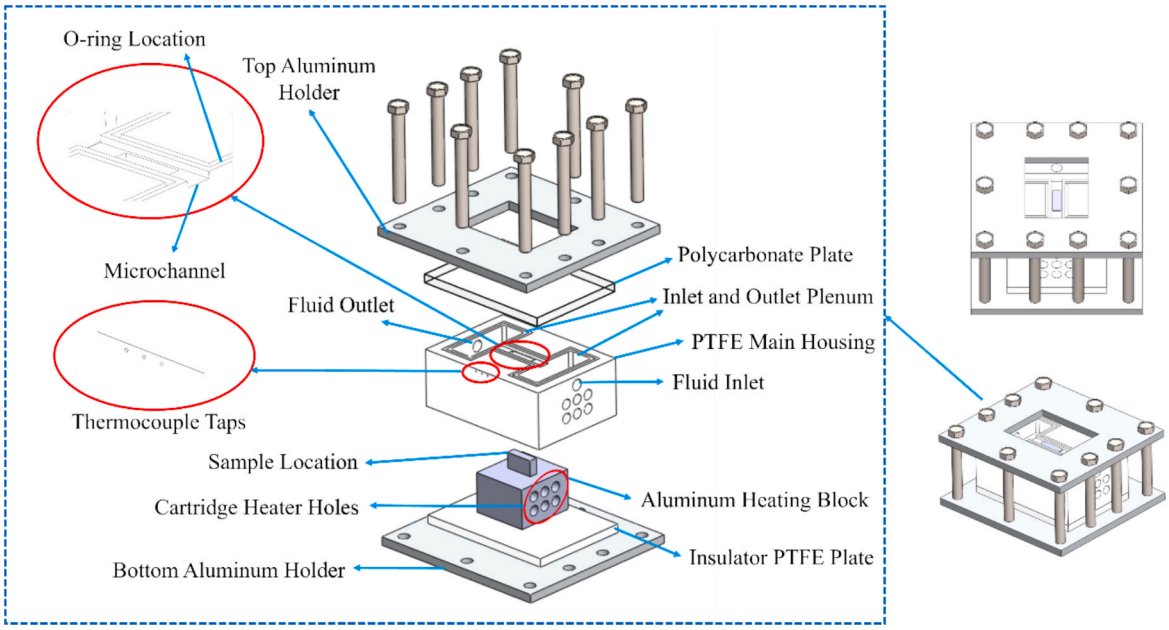

Fig. 4. Detailed view of the rectangular high aspect ratio minichannel test section with heater and thermocouple arrangements.

aluminum block's top surface and the sealing polycarbonate plate forms the minichannel with a depth of 5 mm. Three thermocouple taps were drilled on the main housing along the flow direction at 4 mm beneath the sample and heating block interface at equal distances from each other to measure wall temperature along the channel. The bottom PTFE plate served as an insulator to minimize heat losses. The whole parts of the test section were sandwiched between two aluminum plates to ensure sealing and prevent fluid leakage.

Dielectric HFE-7000 fluid was used as the working fluid and degassed for 24 h at atmospheric pressure. The thermophysical properties of the fluid at atmospheric pressure (1 atm) and room temperature (25 °C) are presented in Table 1. In order to release the dissolved gas and to keep the test pressure close to atmospheric pressure, the vent valve at the top of the reservoir was opened every few minutes during the tests. The flow rate was set to the desired value of 10 L/h by adjusting the needle valve and the input power of the vane pump. The water bath was adjusted to the desired temperature and kept working until it reached the steady state condition to ensure the inlet subcooling of 10 ± 1 ℃ before entering the test section. Inside the test section, the input heating power was increased by raising the input voltage with an increment of 10 V for each heat flux. The temperature and pressure data were recorded until steady-state conditions were obtained for each heat flux.

2.3. Data reduction

The total generated heat by cartridge heaters was calculated by measuring the input electrical power (P):

Table 1
Thermophysical properties of HFE-7000 at atmospheric pressure and room temperature.

Properties	Value
Saturation temperature at 1 atm	34 °C
Liquid density	1376.15 kg.m^{-3}
Vapor density	0.7 kg.m^{-3}
Surface tension of the liquid	58 kN.m^{-1}
Latent heat of vaporization	142 kJ.kg^{-1}
Thermal conductivity	0.075 W.m^{-1}K^{-1}
Liquid viscosity	0.32 mPa.s
Specific heat at constant pressure	1.3 kJ.kg^{-1}K^{-1}

$$P = VI \tag{1}$$

Many studies estimated the heat loss by calculating the ratio of the absorbed heat by the fluid to the total electrical power (φ) from a series of single-phase test results [13]. The effective heat transferred to the surface (q_s) was calculated from single-phase experiment results, which is equal to the deduction of heat losses from the input power:

$$q_s = \dot{m}c_P(T_{out} - T_{in}) = P - q_{loss} \tag{2}$$

$$\varphi = \frac{q_s}{P} \tag{3}$$

where ($\dot{m}$) represents the mass flow rate, and c_P is the specific heat of the working fluid at constant pressure. According to the single-phase heat transfer test results, the φ ranging from 0.85 to 0.9 depending on the applied heat fluxes which correspond to heat loss percentage ranging from 10 % to 15 %.

The effective heat flux was then estimated by calculating the effective heater area (A_e):

$$q''_e = \frac{q_s}{A_e} \tag{4}$$

The effective surface area is the top surface area of the Aluminum heating block, which was 15 × 50 mm^2 in this study. The surface mean temperature is required to calculate the local Heat Transfer Coefficient (HTC). Three temperature measurement points located at 4 mm beneath the substrate along the channel were used to calculate the average surface temperature:

$$T_{avg} = \frac{T_1 + T_2 + T_3}{3} \tag{5}$$

The average single-phase and subcooled heat transfer coefficient (h_{sp}) was obtained from the following equation:

$$h_{sp} = \frac{q''_e}{T_{wall} - T_f} \tag{6}$$

The fluid temperature for single-phase subcooled experiments was calculated from the energy balance, while it is equal to the saturation temperature for saturated boiling ($T_f = T_{sat}$). T_f, is the fluid temperature

(K) for single-phase and subcooled tests and is expressed as:

$$T_{f,x} = T_{in} + \frac{q_e x_{th}}{\dot{m} c_p L_x} \tag{7}$$

where $\dot{m}$, c_p, x_{th}, and L_x are the mass flow rate, specific heat, thermocouple location, and heated length, respectively. For saturated boiling, the two-phase heat transfer coefficient (h_{tp}) is given as:

$$h_{tp} = \frac{q''_e}{T_{wall} - T_{sat}} \tag{8}$$

where T_{wall} is the surface average temperature (K), and T_{sat} is the saturation temperature of the fluid (K).

The one-dimensional heat conduction analysis was used to determine the bottom channel wall temperature:

$$T_{wall} = T_{avg} - q''_e\left(\frac{L_{Al}}{K_{Al}} + \frac{L_{Si}}{k_{Si}} + R_{paste}\right) \tag{9}$$

where R_{paste} is the thermal resistance of a thin layer of thermal paste (6 $\times$ 10^{-6} m^2K/W). L_{Al}, is the vertical distance between the measurement locations and the upper surface of the Aluminum block (4 mm), and L_{Si} is the thickness of the silicon wafer which is 500 μm (Fig. 5). K_{Al} and K_{Si} are the thermal conductivities of Aluminum and Silicon (W/mK), respectively. Also, the vapor quality at exit can be calculated as:

$$x_e = \frac{q_e - \dot{m} c_p (T_{sat} - T_{f,x})}{\dot{m} h_{fg}} \tag{10}$$

2.4. Uncertainty analysis

The uncertainties in the experimental parameters are presented in Table 2. The uncertainty values in measured parameters were obtained from the specification sheets provided by the manufacturers. The uncertainty in the derived experimental parameters was calculated using the propagation of uncertainty analysis method proposed by Coleman and Steele [42].

$$U_p = \sqrt{\sum_{i=1}^{n} \left(\frac{\partial p}{\partial a_i} U_{a_i}\right)^2} \tag{11}$$

where p is the derived parameter, a is the measured parameter, U_{a_i} represents the uncertainty of the measured parameters a_i, and U_p is the uncertainty of the derived parameter p.

The bubble departure diameter for both samples was calculated by taking the average of three diameter measurements along the length of the channel using the captured videos immediately after the departure for a duration of 1.5 to 3 ms. The videos were recorded in full–pixel resolution of 1920 $\times$ 1080 at a frame rate of 3000 fps. An uncertainty of $\pm$ 15 % was obtained due to the error in determining the edge of bubbles and the non-spherical shape of bubbles. The visualization images were post-processed using the ImageJ software to estimate the average bubbles departure diameter.

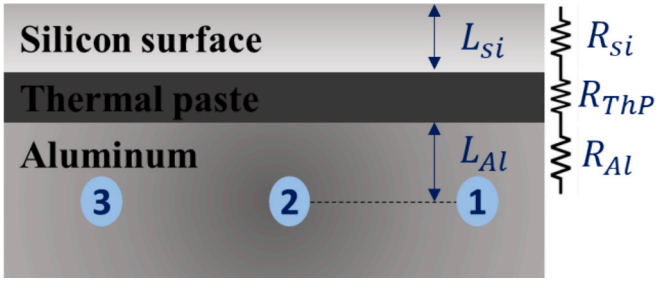

Fig. 5. Three thermocouple locations and schematic of thermal resistances (1-D conduction analysis) to calculate the wall temperature.

Table 2
Uncertainties in experimental parameters.

Parameters	Uncertainty
Inlet Pressure [P_{in}]	±1%
Outlet Pressure [P_{out}]	±0.4 %
Temperature [T]	±1 ℃
Mass Flow Rate [G]	±2.5 %
Dimensions	±15 μm
Voltage [V]	±1V
Current [I]	±0.1A
Two-Phase Heat Transfer Coefficient [h_{tp}]	±7%

2.5. Characterization of bio-coated surface

Microorganisms form biofilms to survive nutrient deficiency, extreme temperatures and different harsh conditions. Similar to bacterial biofilm formation, cells aggregate and adhere to surfaces in archaeal biofilm formation. Irreversibly attached cells form microcolonies and then secrete substances such as glycoproteins, carbohydrates, and DNA. This leads to the formation of multilayered archaeal biofilm [43]. Porous structures form on the biofilm due to the release of gases such as H_2S, CO_2 and SO_2. Our previous study on bio-coatings [40] discussed the effect of incubation temperature on the surface morphology. While the rapid release of H_2S, CO_2, and SO_2 gases from the biofilm at high-temperature incubation generates a porous structure, the incubation at room temperature forms a rough structure. In this study, samples with porous structures were fabricated using the mixed dip coating methodology, which was not considered in the previous study [40] and was also suitable for a scalable preparation for their use in energy systems. Polycation acts as a bridge between the surface of the silicon substrate and *Saccharolobus solfataricus* bio-coating layer with negative charges. The coating attaches to the substrate using electrostatic interactions. Poly-L-Arginine (PLA) bio-polycation provides a more adhesive and more durable coating layer due to higher particle distribution efficiency and charge density compared to Poly-L-Lysine (PLL) [44]. For this reason, in this study, PLA was utilized for polycation. The formation of porous structure and bubble release from the surface was visualized (Fig. 2). After *Saccharolobus solfataricus* cells were fixed on the silicone surface, the surface morphology was visualized by SEM (Scanning Electron Microscopy) (Fig. 6a, b). The SEM analysis proved that the bio-coated silicon surfaces presented a highly porous structure. Porosity of surfaces is a critical parameter which results in a higher heat transfer coefficient due to increased surface area and liquid transfer to nucleation sites [45,46]. In this study, the naturally formed micro- and nano-scale porosity in the biofilm serves as a passive wick, promoting capillary flow towards heated regions and raising the bubble departure frequency through sustained microlayer wetting.

In a study, Xi *et al.* revealed the effect of surface wettability on interfacial heat transfer [47]. They indicated that the hydrogen bond network in hydrophilic surfaces contributed to heat transfer, and the ratio of hydrophilic surface area to hydrophobic surface was closely related to the heat transfer performance. In the current study, the CA measurements were made for the wettability analysis of the bio-coated silicone and plain silicone surfaces (Fig. 7a, b). According to the results of the CA measurements, the bio-coated surface exhibits a hydrophilic behavior with an average CA of 15° relative to the plain silicon surface which has a CA of 61°. In literature, the CA of bare silicon wafer was mentioned as around 33° [48]. However, the water contact angles of the plain silicon surface could increase with the aging time, up till reaching the saturating points of approximately 70° [49]. In addition, the surface profilometer results which are included in Supplementary Information S1 demonstrate that the average thickness of the coating is nearly 5.5 μm.

The structural properties of the bio-coated surfaces, including the porosity, thickness, roughness, and wettability, play a critical role in enhancing flow boiling performance. The porous formation of the

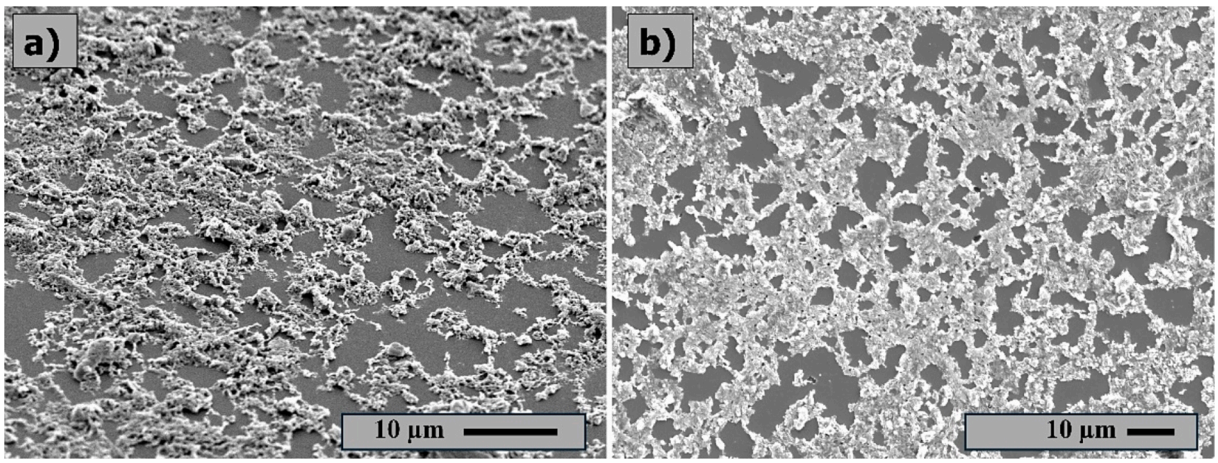

Fig. 6. SEM Results of the bio-coated silicon surface, (a) 45 °C titled image of the coating (scale bar 10 μm) (b) 2D SEM image of the coating (scale bar 10 μm).

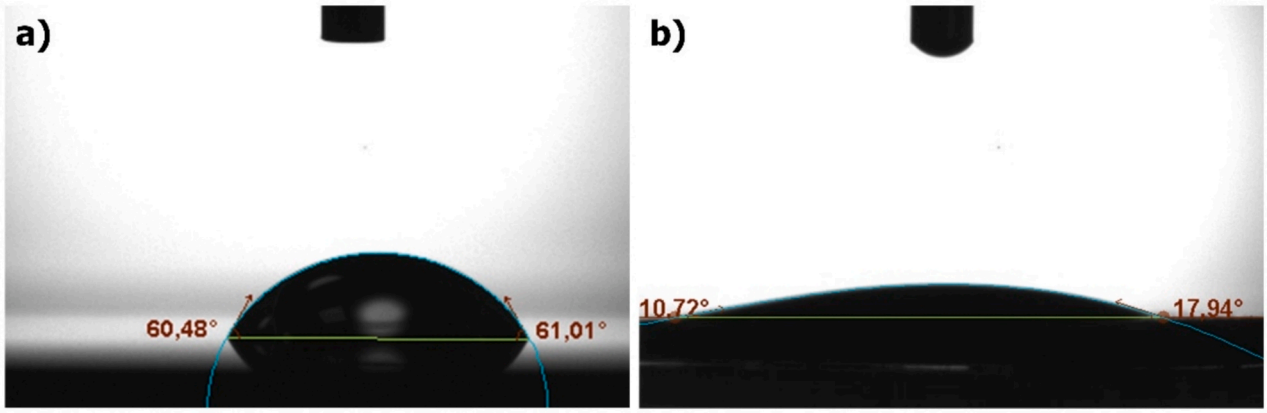

Fig. 7. CA results of the (a) plain silicon surface, (b) bio-coated surface.

coating makes heat transfer more efficient by improving liquid transport to nucleation sites with the increased surface area. The increased polycation concentration results in a large surface roughness, enhancing boiling by creating more active nucleation sites and lowering the temperature required for boiling initiation. The hydrophilic nature of the bio-coated surface allows better liquid expansion and rewetting, which improves heat transfer by promoting bubble detachment and enhancing CHF. Additionally, the hydrophilicity of the bio-coating helps in slowing down the loss of the properties of the surface. In contrast, a plain silicon surface tends to become more hydrophobic over time, which increases the bubble departure diameter, reduces the number of active nucleation sites, and raises the superheat required to initiate boiling. Consequently, these optimized structural properties of the bio-coated surfaces make it an ideal candidate for energy systems by decreasing the thermal resistance, improving boiling stability, and prolonging surface durability.

3. Results and discussion

3.1. Single phase validation

Single-phase experiments were performed before the boiling heat transfer experiments to validate the experimental setup and procedure. The validation experiments were done at the system pressure of 1 atm using DI water in the minichannel with the bare silicon surface for Reynolds numbers ($Re = \frac{\rho u_{av} D_h}{\mu}$) between 580 and 1805. The average Nusselt number (Nu) was calculated according to Shah and London [50] correlation which was recommended for laminar developing flows in horizontal ducts:

$$Nu = 1.953(RePr\frac{D_h}{L})^{\frac{1}{3}} RePr\frac{D_h}{L} \geq 33.3 \quad (12)$$

$$Nu = 4.364 + 0.0722(RePr\frac{D_h}{L}) RePr\frac{D_h}{L} < 33.3 \quad (13)$$

To evaluate the capability of the prediction, the mean absolute error (MAE) was utilized:

$$MAE = \frac{1}{N}\sum_{X=1}^{N}\left|\frac{Nu_{pred} - Nu_{exp}}{Nu_{exp}}\right| \quad (14)$$

Fig. 8 demonstrates the comparison between single-phase experimental results and predictions of the correlation. The proposed correlation by Shah and London could predict the experimental Nu numbers with a MAE of ± 16 %.

3.2. Flow patterns

The bubble nucleation and departure in minichannels are closely related to heat transfer mechanisms. High-speed flow boiling visualization of porous and bare samples was performed at atmospheric pressure P = 1 atm, the mass flux of G = 500 kg/m^{2}s, inlet subcooling of ΔT_{sub} = 10 ℃, and effective heat flux ranges of low (q''_e = 5.4 W/cm^2-12.4 W/cm^2), medium (q''_e = 12.4 W/cm^2-33.9 W/cm^2), and high (q''_e = 33.9 W/cm^2-50.9 W/cm^2). Accordingly, five different flow patterns, namely bubbly, slug, churn, wavy-annular, and annular flow, were

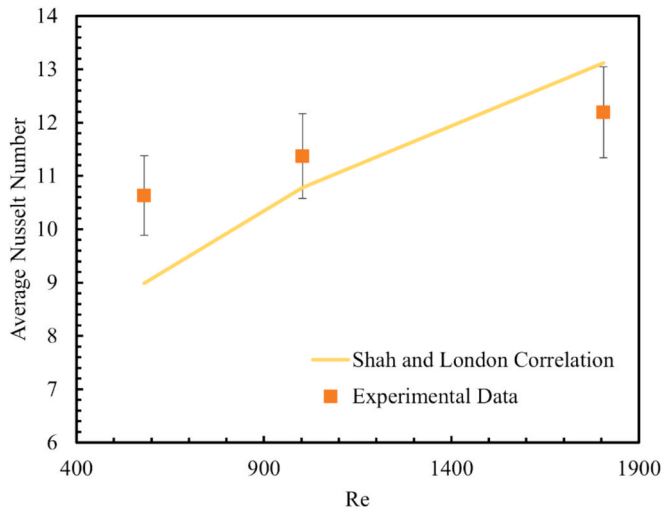

Fig. 8. Single-phase Nusselt number values compared to the predictions of the Shah and London correlation.

detected in the minichannel with the porous surface sample. On the other hand, four flow patterns, namely bubbly, slug, churn, and annular/mist flow, were observed in the channel with the plain surface sample. The flow pattern maps of the channel with a bare silicon surface and the channel with a porous bio-coated surface indicate the transition between the flow patterns along the channel and are shown in Fig. 9a and b, respectively. The length of the channel was divided into 10 equal pieces, and the flow maps were constructed based on the location between the inlet and outlet points and the Boiling number (Bo) defined as $Bo = \frac{q''_e}{Gh_{fg}}$ [4].

Accordingly, the transition between flow patterns happens earlier at a fixed location along the channel for the bio-coated sample compared to the plain surface sample, which is due to more nucleation activity as well as coalescence of emerging bubbles.

The flow images in Fig. 10 cover the entire length of the channel. Bubbly flow is first detected in the low heat flux range at a lower heat flux of 5.4 W/cm^2 on the bio-coated surface compared to the bare silicon surface sample, characterized by individual bubbles that depart from the surface of the sample with smaller departure diameters (Fig. 10). Uniformly distributed isolated bubbles can represent bubbly flow in the low heat flux range, as shown in Fig. 10b. The bubbly flow is extended until high heat fluxes at locations close to the inlet of the channel with the bio-coated surface sample. Most nucleation sites are distributed on the coated part of the surface rather than on the sidewalls for the coated sample. The bubbly flow transitions to slug flow along the channel due to the bubble coalescence and larger bubble departure diameters in the channel with the bare silicon surface. Slug flow is detected in the range of medium heat fluxes near the outlet of the coated channel due to bubble coalescence, forming large bubbles separated by a thin liquid film from the side walls of the channel, as shown in Fig. 10b. The slug flow in the plain channel can be clearly observed; however, in the coated channel, continuously nucleated bubbles from the surface of the porous sample penetrate the flow and disturb the slug bubble, which results in the formation of the slug-churn flow pattern at the heat flux of 33.9 W/cm^2 (Fig. 10b). As the heat flux is increased to higher values, a wavy pattern appears at the center of the channel with the porous surface due to the bubble collapse, and a vapor core surrounded by a wavy thin liquid layer becomes visible, which is characterized as a wavy-annular flow as shown in Fig. 10b. Eventually, the annular flow is characterized by the presence of a vapor core surrounded by thin liquid layers on the sidewalls at the high heat flux range. Transition to annular flow and heat transfer via thin film evaporation enhances heat transfer at high heat fluxes. Although bubbles form a churn flow at the inlet of the

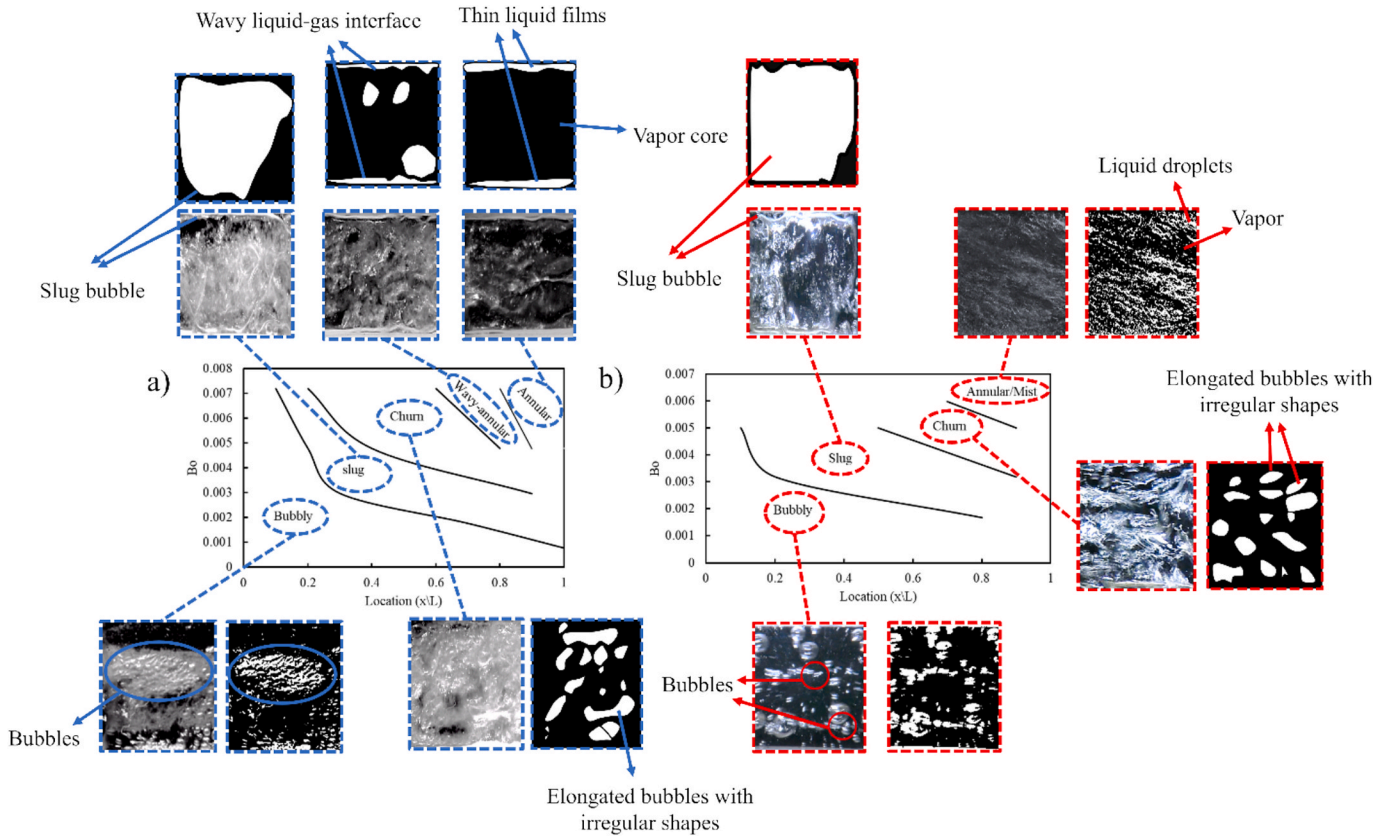

Fig. 9. Flow regime map for the channel with (a) porous bio-coated sample, and (b) bare silicon surface.

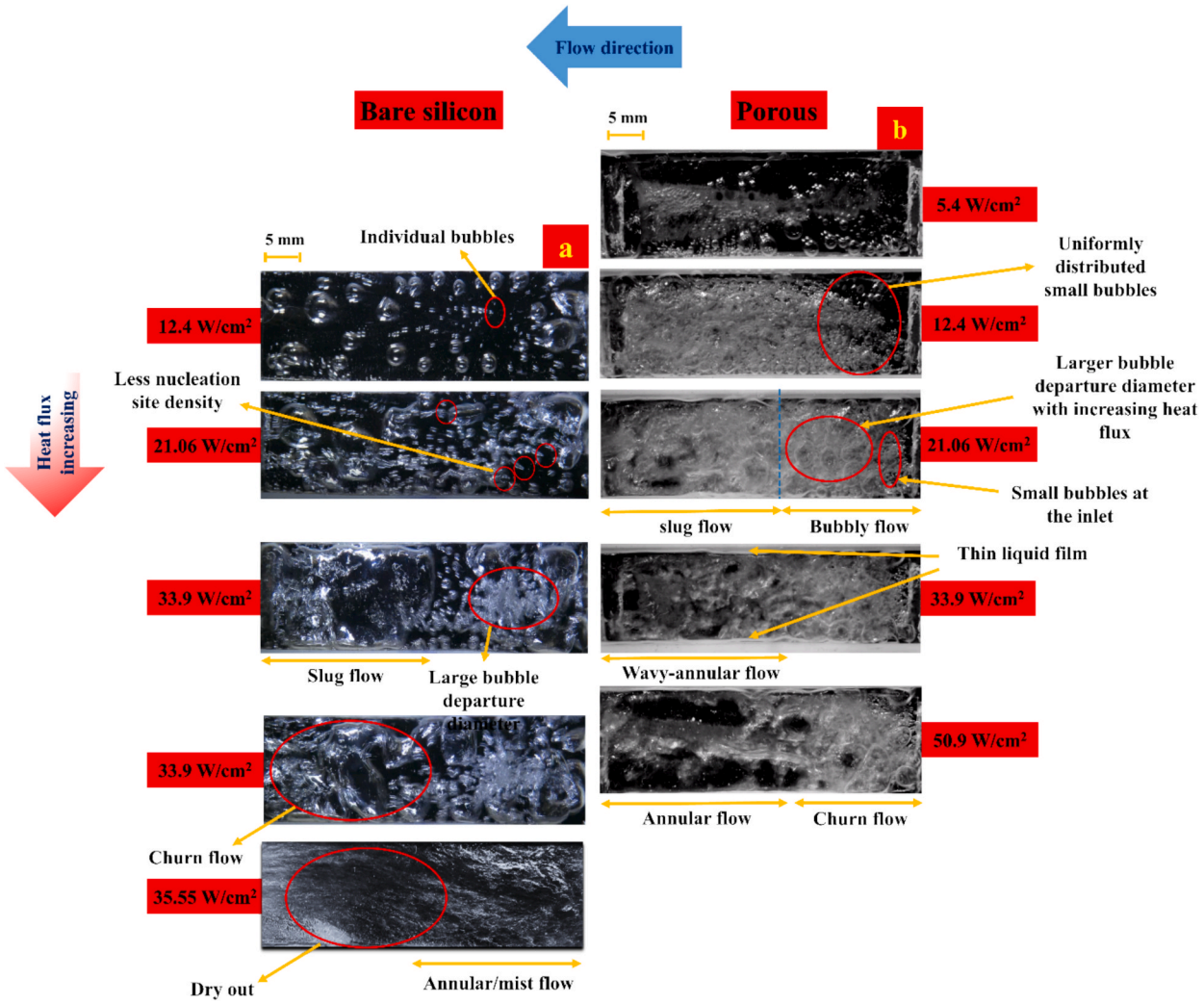

Fig. 10. Flow pattern evolution for (a) bare silicon sample (b) porous bio-coated surface sample at the mass flux of 500 kg/m^{2}s and at different heat fluxes.

channel with the porous sample at the high heat flux of 50.9 W/cm^2, in a channel with the plain sample, an annular/mist flow is formed by liquid droplets with small diameters flowing inside a vapor core.

Fig. 11 illustrates the process of bubble nucleation and coalescence at the heat flux of 12.4 W/cm^2, highlighting the formation of slug flow. The bubbles emerge on the coated section of the channel. As the bubbles merge from both the channel sides and the coated surface (marked in red), their diameter grows, eventually leading to slug formation.

3.3. Bubble departure diameter

Bubble nucleation starts earlier for the coated sample (Fig. 9). In the bubbly flow regime, isolated bubbles with a size smaller than the width of the channel depart from the sidewalls and surface. The porosity of bio-coating due to the bio-polycation leads to more bubble nucleation activity from the porous medium, which facilitates heat transfer from the surface to the fluid. Moreover, the smaller and more frequent bubble departures reduce the thermal boundary layer thickness and maintain a more uniform wall temperature distribution, contributing to the overall enhancement in heat transfer performance. Furthermore, the porous structure with more surface area also offers more nucleation sites.

The bubble departure diameter is a major parameter affecting boiling heat transfer. It is obvious from Fig. 12a,b that the nucleation site density and bubble departure diameter are different for the coated sample compared to the bare silicon surface sample at low and high heat fluxes. Smaller bubbles (smaller bubble departure diameter) compared to plain surfaces are homogenously distributed on the porous surface with a uniform bubble size at a fixed heat flux of $q''_e = 12.4$ W/cm^2 (Fig. 12a, Fig. 13). Larger bubble departure diameters along with fewer bubble nucleation sites can be seen on the bare silicon surface at the same heat flux. For both of the samples, a small bubble departure diameter was detected compared to the experiments with water [40] due to the low liquid-to-vapor density ratio and low surface tension of HFE-7000. Bubble departure diameter was measured at different heat fluxes for the bare and porous surfaces near the inlet region where bubble flow exists.

3.4. Heat transfer enhancement

The boiling curves for bio-coated and bare silicon surfaces are depicted in Fig. 13. In the low heat flux region, the boiling curves are close to each other, which suggests that the coated sample does not offer much heat transfer enhancement. Upon increasing the heat flux, the bio-coated surface starts to outperform the bare silicon, and their boiling curves tend to diverge, which is linked with heat transfer enhancement by means of bio-coated surfaces at higher heat fluxes. The porous structure of the bio-coating material with interconnected pore networks and its hydrophilicity nature enables surface rewetting and delays the vapor blanket formation at high heat fluxes. This promotes efficient thin film evaporation in annular regimes, where a stable liquid layer is

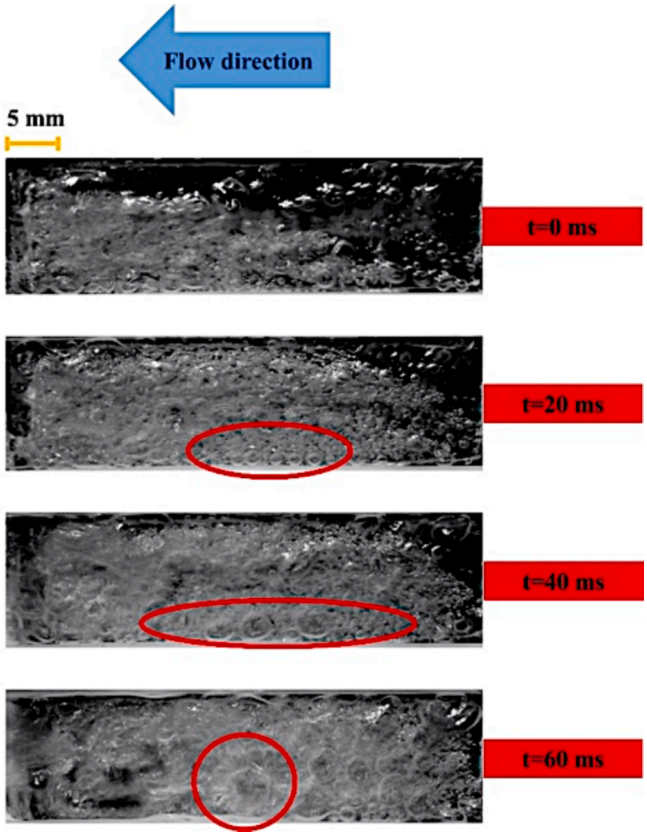

Fig. 11. Flow pattern evolution (to slug flow) in the porous coated channel.

maintained over the porous matrix, enhancing heat removal through a phase change and suppressing the dryout phenomenon. In addition, numerous heterogeneous nucleation sites provided by the coated sample lead to higher bubble generation potential and better heat removal at medium heat fluxes.

To evaluate the heat transfer enhancement with the proposed porous bio-coating, the heat transfer coefficients (HTC) of the coated sample are compared to the bare silicon surface in Fig. 14. The decreasing trend in HTC as a function of wall heat flux happens due to the prevalence of slug and annular flows at higher heat fluxes, which agrees with the literature on convective flow boiling [9]. The bio-coated surface sample demonstrates notable maximum enhancements in HTCs (50 %) compared to the bare silicon sample. This enhancement significantly outperforms the previously introduced porous coating structures. In a previous study of the flow boiling of HFE-7200 in a heat sink with a porous coating that was applied to the channel by micro milling, a 44 % enhancement in HTC was achieved at low heat fluxes, which decreased to 13 % at high heat fluxes due to the suppression of nucleate boiling [51]. Furthermore, in a recent study on the flow boiling in chemically etched porous copper tubes, a maximum enhancement of 41 % in HTC was reported [26]. The enhancement mechanism is illustrated in Fig. 15, highlighting the boiling dynamics enabled by the bio-coated surface.

The dominant heat transfer mechanism for both bare silicon and bio-coated samples is nucleate boiling at a low heat flux range. The presence of more nucleation sites with smaller bubbles in the channel with a bio-coated sample (shown in Fig. 15) enhances heat transfer. The interconnected channels in the porous structure of bio-coating enhance the vapor escape from the surface and the rewetting process by surrounding liquid. This dual function of vapor venting and liquid supply results in a self-regulating thermal interface, where bubble departure is less disruptive, and boiling instabilities are minimized, particularly in the transition and annular flow regimes. Therefore, more nucleation sites exist on the bio-coated sample, while the bubble release frequency is also higher for this surface. Consequently, heat transfer is improved by more nucleation activity and higher bubble release frequency from the surface.

Upon an increase in heat flux to a higher value, the transition to annular flow, where a thin liquid film surrounded by the vapor phase forms on the channel walls, occurs. Heat transfer is enhanced in the bio-coated channel compared to the channel with a bare silicon surface via effective thin film evaporation on the porous surface, which sustains the liquid film at the high heat flux range. On the other hand, large-size bubbles and bubble coalescence in the channel with bare silicon sample lead to dry-out conditions/ dry spots in the high heat flux range. The related heat transfer mechanisms are summarized in Fig. 15.

CHF (Critical heat flux) is another parameter that determines the applicability of bio-coatings to industrial applications. In the literature,

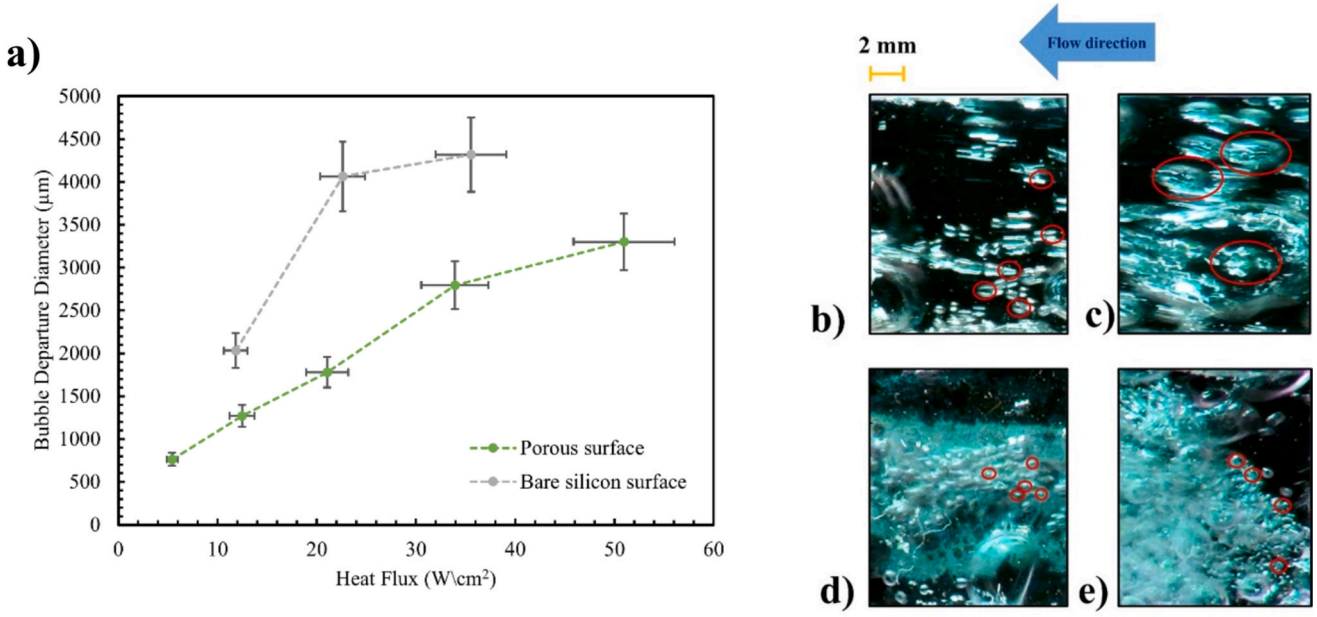

Fig. 12. (a) Bubble departure diameter as a function of heat flux for both bare silicon and porous surfaces. Images of bubble departure for the bare silicon surface at heat fluxes of (b) 12.4 W/cm^2 and (c) 33.9 W/cm^2, and for the porous surface at heat fluxes of (d) 12.4 W/cm^2 and (e) 33.9 W/cm^2.

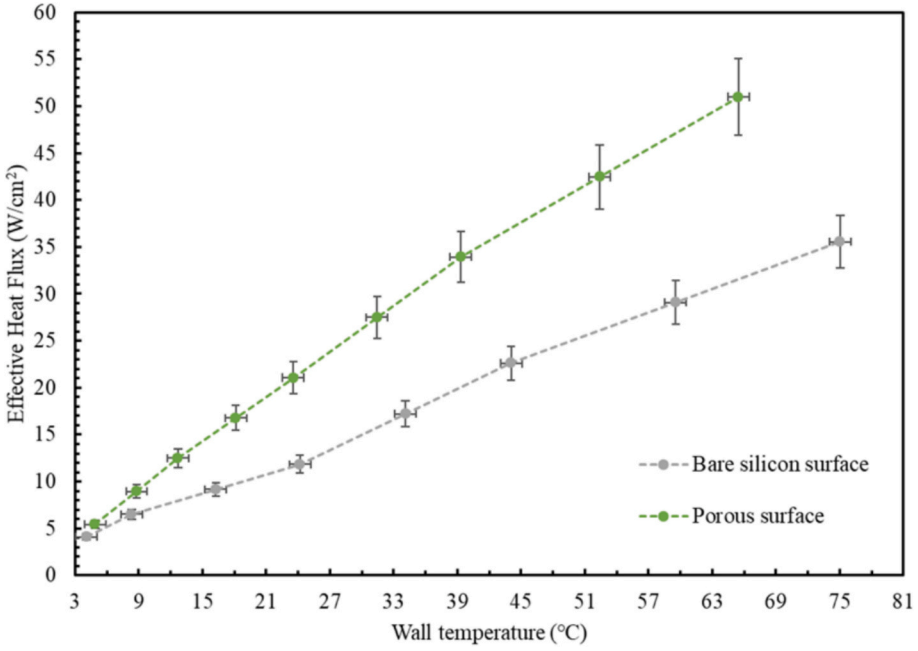

Fig. 13. Comparison between wall superheats with respect to the heat flux for porous and bare silicon samples.

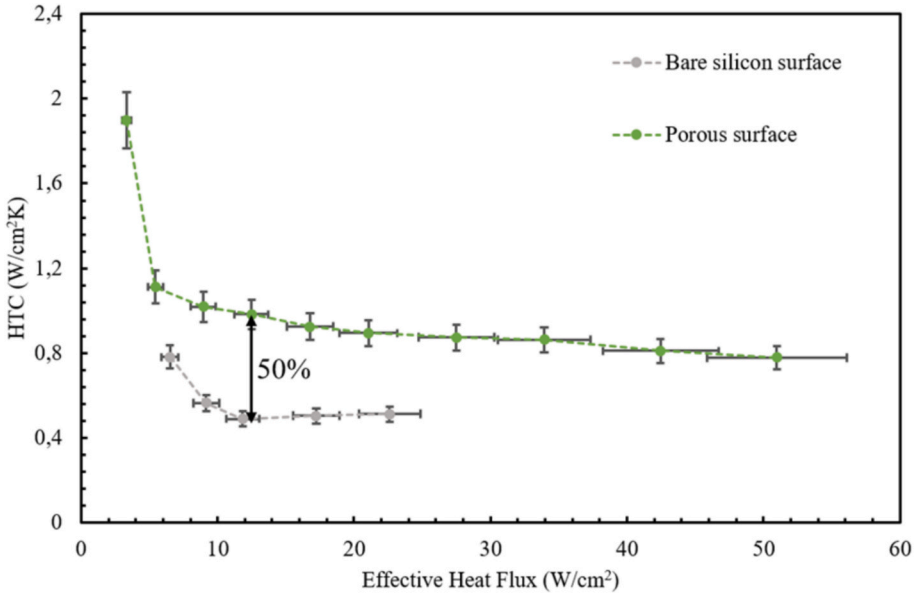

Fig. 14. Heat transfer coefficient enhancement at mass flux of 500 kg/m^{2}s.

it was reported that porous coatings delay CHF by the rewetting process of the hotspots, which feeds the liquid to the pores and removes bubbles [52]. Empirical models developed using extensive datasets can successfully predict CHF under different conditions. One of the most widely used correlations for predicting the CHF of the flow boiling of various fluids in a single channel with different geometries is the one developed by Katto and Ohno [53]. Accordingly, the Katto and Ohno correlation for sub-cooled boiling conditions is expressed as:

$$q_{CHF} = q_{sat}(1 + \frac{K\Delta h_{in}}{h_{fg}}) \tag{15}$$

where q_{CHF} is the CHF corresponding to the sub-cooled condition, q_{sat} is the CHF corresponding to the saturated boiling condition, K is the inlet subcooling parameter, h_{fg} is the latent heat of evaporation, and Δh_i is the inlet subcooling enthalpy, and is calculated as:

$$\Delta h_{in} = c_p(T_{sat} - T_{in}) \tag{16}$$

q_{sat} is calculated for flow boiling as:

$$q_{sat} = Gh_{fg}.0.098\left(\frac{\rho_v}{\rho_l}\right)^{0.133}.\left(\frac{\sigma\rho_l}{G^2 l}\right)^{0.433}.\frac{\left(\frac{l}{d_h}\right)^{0.27}}{1 + 0.0031(\frac{l}{d_h})} \tag{17}$$

where l is the heated length and K is found as:

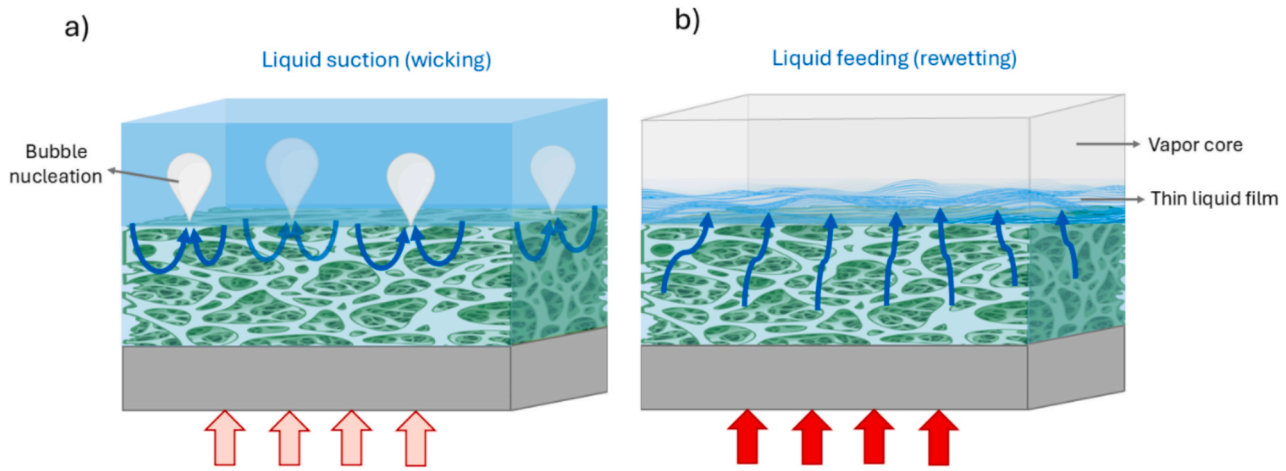

Fig. 15. Heat transfer enhancement mechanisms on bio-coated surfaces (a) at low and (b) high heat flux ranges.

$$K = 0.416 \frac{\left(0.0221 + \frac{d_h}{l}\right)\left(\frac{d_h}{l}\right)^{0.27}}{\left(\frac{\rho_v}{\rho_l}\right)^{0.133}\left(\frac{\sigma\rho_l}{G^2 l}\right)^{0.433}} \quad (18)$$

Accordingly, the experimental CHF values, which were considered as the last heat flux value of the boiling curve for the bare silicon and porous-coated samples where permanent dryout locations started to appear, and the predicted CHF value corresponding to a plain surface are demonstrated in Table 3.

A small Mean Absolute Error (1.63 %) between the experimental CHF value of the plain sample and the prediction of the Katto and Ohno correlation, a widely used correlation for flow boiling, exists. Furthermore, the ratio of the experimental CHF value with porous bio-coatings to that of the plain surface, which is also defined as the enhancement factor, is about 1.5. This enhancement is attributed to the hydrophilicity as well as the capillary wicking capability of the porous bio-coated samples (Fig. 15), where the coating structure prevents the formation of the vapor blanket on the surface at high heat fluxes, thereby delaying the dryout and CHF condition.

4. Conclusion

Flow boiling heat transfer of the dielectric fluid HFE-7000 was investigated in a rectangular minichannel with 50 × 15 × 5 mm^3 dimensions and a porous bio-coated silicon sample. The tested bio-coating was a proposed environmentally friendly and economical microbial bio-coating and was prepared using the scalable dip-mixed coating method. The tests were performed at a mass flux of 500 kg/m^2 s and a subcooling degree of 10 ℃. The heat transfer enhancement mechanisms were discussed in light of flow visualization. The main findings are summarized as:

- The porous bio-coated sample results in a better performance in terms of HTC and wall temperature compared to the plain silicon surface and proves that bio-coatings are effective in enhancing the boiling heat transfer of dielectric fluids with smaller surface tension and latent heat of vaporization. This enhancement arises from a synergy of increased nucleation site density, hydrophilic microlayer stabilization, and capillary-driven rewetting, which collectively address the major limitations of dielectric fluids under high heat flux conditions.
- The maximum enhancement in two-phase HTC (50 %) was attributed to porous coating, which provided surface rewetting and enhanced thin film evaporation at high heat fluxes (q''_e = 33.9 W/cm^2-50.9 W/cm^2) and more nucleation sites and more frequent release of smaller bubbles at low heat fluxes (q''_e = 5.4 W/cm^2-12.4 W/cm^2).
- A 50 % increase in CHF was obtained after applying the bio-coating to the plain sample, due to the prevention of vapor blanket formation by the porous bio-coating.
- A smaller bubble departure diameter was observed in channels with porous coated surfaces compared to plain samples and experiments with water, due to the low surface tension of HFE-7000 and the favourable effects of the coating.
- Earlier transition between flow patterns was observed in the channel with the bio-coated surface sample compared to the bare silicon surface due to the higher nucleation site density at low heat fluxes and effective thin film evaporation in annular flow at high heat fluxes.

Table 3
Comparison of the CHF values with Katto and Ohno [53] correlation.

$q_{CHF,Katto}$ (W/cm^2)	$q_{CHF,\ plain}$(W/cm^2)	$q_{CHF,\ porous}$(W/cm^2)	MAE(%)
34.97	35.55	50.98	1.63

In this study, flow boiling heat transfer could be enhanced in flow boiling of the HFE-7000 dielectric fluid by using an eco-friendly bio-coating with a porous structure, which can promote bubble nucleation, surface rewetting, and thin film evaporation. Further studies are needed to investigate the effect of the coating thickness on the flow boiling heat transfer performance. Furthermore, the long-term durability of the coating under high-speed flows and the long-term sustainability of enhanced performance of bio-coated surfaces constitute other future research directions.

CRediT authorship contribution statement

Mandana Mohammadilooey: Writing – original draft, Visualization, Validation, Software, Methodology, Data curation. **Zülal Muganlı:** Investigation, Formal analysis, Data curation. **Soroush Niazi:** Software, Resources, Methodology, Investigation. **Gül Kozalak:** Writing – review & editing, Writing – original draft, Resources, Methodology, Investigation. **Erçil Toyran:** Visualization, Software, Investigation, Data curation. **Hyun Sun Park:** Writing – review & editing, Writing – original draft, Supervision, Resources, Funding acquisition. **Ali Sadaghiani:** Writing – review & editing, Writing – original draft, Project administration, Investigation. **Ali Koşar:** Writing – review & editing, Writing – original draft, Supervision, Project administration, Methodology, Funding acquisition, Conceptualization.

Declaration of competing interest

The authors declare that they have no known competing financial interests or personal relationships that could have appeared to influence the work reported in this paper.

Acknowledgement

The authors appreciate the support by TUBITAK (The Scientific and Technological Research Council of Turkey) Support Program for Scientific and Technological Research Projects grant number 119C026, and the European Commission in Micro-FloTec project (101082384) under Horizon Europe MSCA Staff Exchanges.

Data availability

Data will be made available on request.

References

[1] The semiconductor decade: A trillion-dollar industry, 2022.
[2] A. Bar-Cohen, C.A. Holloway, Thermal science and engineering - from macro to nano in 200 years, In (2014). https://api.semanticscholar.org/CorpusID:138161526.
[3] H. Honda, J. Wei, Advances in enhanced boiling heat transfer from electronic components, JSME Int J., Ser. B 46 (2003) 479–490, https://doi.org/10.1299/jsmeb.46.479.
[4] T. Harirchian, S.V. Garimella, Effects of channel dimension, heat flux, and mass flux on flow boiling regimes in microchannels, Int. J.Multiph. Flow 35 (2009) 349–362, https://doi.org/10.1016/j.ijmultiphaseflow.2009.01.003.
[5] X. Hu, G. Lin, Y. Cai, D. Wen, Experimental study of flow boiling of FC-72 in parallel minichannels under sub-atmospheric pressure, Appl. Therm. Eng. 31 (2011) 3839–3853, https://doi.org/10.1016/j.applthermaleng.2011.07.032.
[6] A. Aboubakri, V.E. Ahmadi, S. Celik, A.K. Sadaghiani, K. Sefiane, A. Kosar, Effect of surface biphilicity on FC-72 flow boiling in a rectangular minichannel, Front. Mech. Eng. (2021) 95, https://doi.org/10.3389/FMECH.2021.755580.
[7] Y.-F. Wang, J.-T. Wu, Thermal performance predictions for an HFE-7000 direct flow boiling cooled battery thermal management system for electric vehicles, Energy Convers Manag 207 (2020) 112569, https://doi.org/10.1016/j.enconman.2020.112569.
[8] M.S. El-Genk, M. Pourghasemi, Experimental investigation of saturation boiling of HFE-7000 dielectric liquid on rough copper surfaces, Therm. Sci. Eng. Prog. 15 (2020) 100428, https://doi.org/10.1016/j.tsep.2019.100428.
[9] M. Piasecka, K. Strąk, Characteristics of refrigerant boiling heat transfer in rectangular mini-channels during various flow orientations, Energies (basel) 14 (2021), https://doi.org/10.3390/en14164891.
[10] U. Sajjad, A. Sadeghianjahromi, H.M. Ali, C.-C. Wang, Enhanced pool boiling of dielectric and highly wetting liquids - a review on enhancement mechanisms, Int. Commun. Heat Mass Transfer 119 (2020) 104950, https://doi.org/10.1016/j.icheatmasstransfer.2020.104950.
[11] B.P. Benam, V.E. Ahmadi, A.R. Motezakker, S. Saeidiharzand, L.G. Villanueva, H. S. Park, A.K. Sadaghiani, A. Koşar, A parametric study on pool boiling heat transfer and critical heat flux on structured surfaces with artificial cavities, Appl. Therm. Eng. 221 (2023) 119841, https://doi.org/10.1016/J.APPLTHERMALENG.2022.119841.
[12] A.K. Sadaghiani, N.S. Saadi, S.S. Parapari, T. Karabacak, M. Keskinoz, A. Koşar, Boiling heat transfer performance enhancement using micro and nano structured surfaces for high heat flux electronics cooling systems, Appl. Therm. Eng. 127 (2017) 484–498, https://doi.org/10.1016/j.applthermaleng.2017.08.018.
[13] Z. Yao, Y.-W. Lu, S.G. Kandlikar, Effects of nanowire height on pool boiling performance of water on silicon chips, Int. J. Therm. Sci. 50 (2011) 2084–2090, https://doi.org/10.1016/j.ijthermalsci.2011.06.009.
[14] E. Demir, T. Izci, A.S. Alagoz, T. Karabacak, A. Koşar, Effect of silicon nanorod length on horizontal nanostructured plates in pool boiling heat transfer with water, Int. J. Therm. Sci. 82 (2014) 111–121, https://doi.org/10.1016/j.ijthermalsci.2014.03.015.
[15] A.K. Sadaghiani, A.R. Motezakker, S. Kasap, I.I. Kaya, A. Koşar, Foamlike 3D graphene coatings for cooling systems involving phase change, ACS Omega 3 (2018) 2804–2811, https://doi.org/10.1021/acsomega.7b02040.
[16] A.K. Sadaghiani, A.R. Motezakker, A.V. Özpınar, G.O. Ince, A. Koşar, Pool boiling heat transfer characteristics of inclined pHEMA-coated surfaces, Journal of Heat Transfer-Transactions of the Asme 139 (2017) 111501. https://api.semanticscholar.org/CorpusID:125653206.
[17] M.M. Rahman, E. Ölçeroğlu, M. McCarthy, Scalable Nanomanufacturing of Virus-templated Coatings for Enhanced Boiling, Adv. Mater. Interfaces 1 (2014) 1300107, https://doi.org/10.1002/admi.201300107.
[18] A.R. Motezakker, A.K. Sadaghiani, S. Çelik, T. Larsen, L.G. Villanueva, A. Koşar, Optimum ratio of hydrophobic to hydrophilic areas of biphilic surfaces in thermal fluid systems involving boiling, Int. J. Heat Mass Transf. 135 (2019) 164–174, https://doi.org/10.1016/j.ijheatmasstransfer.2019.01.139.
[19] M. Može, M. Senegačnik, P. Gregorčič, M. Hočevar, M. Zupančič, I. Golobič, Laser-Engineered Microcavity Surfaces with a Nanoscale Superhydrophobic Coating for Extreme Boiling Performance, ACS Appl. Mater. Interfaces 12 (2020) 24419–24431, https://doi.org/10.1021/acsami.0c01594.
[20] H. Bostanci, V.P. Singh, J.P. Kizito, D.P. Rini, S. Seal, L. Chow, Microscale surface modifications for heat transfer enhancement., ACS Appl Mater Interfaces 5 19 (2013) 9572–8. https://api.semanticscholar.org/CorpusID:8530549.
[21] B. Parizad Benam, A.K. Sadaghiani, V. Yağcı, M. Parlak, K. Sefiane, A. Koşar, Review on high heat flux flow boiling of refrigerants and water for electronics cooling, Int J Heat Mass Transf 180 (2021), https://doi.org/10.1016/j.ijheatmasstransfer.2021.121787.
[22] W. Wu, H. Bostanci, L.C. Chow, Y. Hong, M. Su, J.P. Kizito, Nucleate boiling heat transfer enhancement for water and FC-72 on titanium oxide and silicon oxide surfaces, Int. J. Heat Mass Transf. 53 (2010) 1773–1777, https://doi.org/10.1016/j.ijheatmasstransfer.2010.01.013.
[23] R. Khodabandeh, R. Furberg, Heat transfer, flow regime and instability of a nano- and micro-porous structure evaporator in a two-phase thermosyphon loop, Int. J. Therm. Sci. 49 (2010) 1183–1192. https://api.semanticscholar.org/CorpusID:122192775.
[24] G. Liang, I. Mudawar, Review of nanoscale boiling enhancement techniques and proposed systematic testing strategy to ensure cooling reliability and repeatability, Appl. Therm. Eng. 184 (2021) 115982, https://doi.org/10.1016/j.applthermaleng.2020.115982.
[25] S.B. White, A.J. Shih, K.P. Pipe, Boiling surface enhancement by electrophoretic deposition of particles from a nanofluid, Int. J. Heat Mass Transf. 54 (2011) 4370–4375, https://doi.org/10.1016/j.ijheatmasstransfer.2011.05.008.
[26] M.J. Inanlu, V. Ganesan, N.V. Upot, C. Wang, Z. Suo, K.F. Rabbi, P. Kabirzadeh, A. Bakhshi, W. Fu, T.S. Thukral, V. Belosludtsev, J. Li, N. Miljkovic, Unveiling the fundamentals of flow boiling heat transfer enhancement on structured surfaces, Sci. Adv. 10 (2024) eadp8632, https://doi.org/10.1126/sciadv.adp8632.
[27] C. Lee, B. Zhang, K. Kim, Morphological change of plain and nano-porous surfaces during boiling and its effect on nucleate pool boiling heat transfer, Exp. Therm Fluid Sci. 40 (2012) 150–158, https://doi.org/10.1016/j.expthermflusci.2012.02.011.
[28] N.V. Upot, K. Fazle Rabbi, S. Khodakarami, J.Y. Ho, J. Kohler Mendizabal, N. Miljkovic, Advances in micro and nanoengineered surfaces for enhancing boiling and condensation heat transfer: a review, Nanoscale Adv. 5 (2023) 1232–1270, https://doi.org/10.1039/D2NA00669C.
[29] G. Longoni, D. Assanelli, C. Marco, Wet Etching and Cleaning, in (2022) 259–292, https://doi.org/10.1007/978-3-030-80135-9_9.
[30] B. Dikici, B. Al-Sukaini, Comparisons of Structured Surface Floors for Pool Boiling Enhancement at Low Heat Fluxes: Hands-on Learning Setup for Heat Transfer Classroom 11 (2023) 303–318, https://doi.org/10.4236/wjet.2023.112022.
[31] B.-Y. Liu, J. Wu, C.-H. Xue, Y. Zeng, J. Liang, S. Zhang, M. Liu, C.-Q. Ma, Z. Wang, G. Tao, Bioinspired superhydrophobic all-in-one coating for adaptive thermoregulation, Adv. Mater. 36 (2024) 2400745, https://doi.org/10.1002/adma.202400745.
[32] Q. Guo, Z. Liu, Z. Yang, Y. Jiang, Y. Sun, J. Xu, W. Zhao, W. Wang, W. Wang, Q. Ren, C. Shu, Development, challenges and future trends on the fabrication of micro-textured surfaces using milling technology, J. Manuf. Process. 126 (2024) 285–331, https://doi.org/10.1016/j.jmapro.2024.07.112.
[33] S. Niazi, A.K. Sadaghiani, G. Gharib, V.O. Kaya, S. Çelik, Ö. Kutlu, A. Koşar, Bio-coated surfaces with micro-roughness and micro-porosity: next generation coatings for enhanced energy efficiency, Energy 222 (2021) 119959, https://doi.org/10.1016/j.energy.2021.119959.
[34] A. Duman, S. Niazi, G. Gharib, A.K. Sadaghiani, A. Koşar, Self-assembled archaea bio-coatings in thermal-fluids systems: a study on adhesion optimization and energy efficiency, International Journal of Thermofluids 15 (2022) 100170, https://doi.org/10.1016/j.ijft.2022.100170.
[35] M. Ciaramella, R. Cannio, M. Moracci, F.M. Pisani, M. Rossi, Molecular biology of extremophiles, World J. Microbiol. Biotechnol. 11 (1995) 71–84, https://doi.org/10.1007/BF00339137.
[36] H.D. Sakai, N. Kurosawa, Saccharolobus caldissimus gen. nov., sp. nov., a facultatively anaerobic iron-reducing hyperthermophilic archaeon isolated from an acidic terrestrial hot spring, and reclassification of Sulfolobus solfataricus as Saccharolobus solfataricus comb. nov. and Sulfolobus shibatae as Saccharolobus shibatae comb. nov, Int. J. Syst. Evol. Microbiol. 68 (2018) 1271–1278, https://doi.org/10.1099/ijsem.0.002665.
[37] L. Čuboňová, K. Sandman, S.J. Hallam, E.F. Delong, J.N. Reeve, Histones in Crenarchaea, J Bacteriol 187 (2005) 5482–5485. https://api.semanticscholar.org/CorpusID:35143945.
[38] B. Chaban, S. Ng, K. Jarrell, Archaeal habitats - from the extreme to the ordinary, Can. J.Microbiol. 52 (2006) 73–116, https://doi.org/10.1139/w05-147.
[39] D.W. Grogant, Phenotypic Characterization of the Archaebacterial Genus Sulfolobus, Comparison of Five Wild-Type Strains (1989).
[40] S. Niazi, A.K. Sadaghiani, G. Gharib, V.O. Kaya, S. Çelik, Ö. Kutlu, A. Koşar, Bio-coated surfaces with micro-roughness and micro-porosity: next generation coatings for enhanced energy efficiency, Energy 222 (2021), https://doi.org/10.1016/j.energy.2021.119959.
[41] A.R. Motezakker, A.K. Sadaghiani, Y. Akkoc, S.S. Parapari, D. Gözüaçlk, A. Koşar, Surface modifications for phase change cooling applications via crenarchaeon Sulfolobus solfataricus P2 bio-coatings, Scientific Reports 2017 7:1 7 (2017) 1–9. DOI: 10.1038/s41598-017-18192-2.
[42] H.W. Coleman, W.G. Steele, Experimentation, Validation, and Uncertainty Analysis for Engineers, in: Experimentation, Validation, and Uncertainty Analysis for Engineers, Wiley, 2009. DOI: 10.1002/9780470485682.fmatter.

[43] M. van Wolferen, A. Orell, S.-V. Albers, Archaeal biofilm formation, Nat. Rev. Microbiol. 16 (2018) 699–713, https://doi.org/10.1038/s41579-018-0058-4.
[44] M. Kar, N. Tiwari, M. Tiwari, M. Lahiri, S. Sen Gupta, Poly-L-Arginine Grafted Silica Mesoporous Nanoparticles for Enhanced Cellular Uptake and their Application in DNA delivery and Controlled Drug Release, Part. Part. Syst. Charact. 30 (2013) 166–179, https://doi.org/10.1002/ppsc.201200089.
[45] Y. Huo, M. Yin, Z. Rao, Heat transfer enhanced by angle-optimized fan-shaped porous medium in phase change thermal energy storage system at pore scale, Int. J. Therm. Sci. 172 (2022) 107363, https://doi.org/10.1016/j.ijthermalsci.2021.107363.
[46] M. Moayeri, A. Kaflou, Effect of powder shape on effective thermal conductivity of Cu–Ni porous coatings, J. Mater. Res. Technol. 7 (2018) 403–409, https://doi.org/10.1016/j.jmrt.2016.12.003.
[47] B. Xi, T. Zhao, Q. Gao, Z. Wei, S. Zhao, Surface wettability effect on heat transfer across solid-water interfaces, Chem. Eng. Sci. 254 (2022) 117618, https://doi.org/10.1016/j.ces.2022.117618.
[48] M.G. Kibria, F. Zhang, T.H. Lee, M.J. Kim, M.M.R. Howlader, Comprehensive investigation of sequential plasma activated Si/Si bonded interfaces for nano-integration on the wafer scale, Nanotechnology 21 (2010) 134011, https://doi.org/10.1088/0957-4484/21/13/134011.
[49] X.M. Yang, Z.W. Zhong, E.M. Diallo, Z.H. Wang, W.S. Yue, Silicon wafer wettability and aging behaviors: Impact on gold thin-film morphology, Mater. Sci.Semicond. Process. 26 (2014) 25–32, https://doi.org/10.1016/j.mssp.2014.03.044.
[50] R.K. Shah, A.L. London, Chapter III - Dimensionless groups and Generalized Solutions, in: R.K. Shah, A.L. London (Eds.), Laminar Flow Forced Convection in Ducts, Academic Press, 1978, pp. 37–60, https://doi.org/10.1016/B978-0-12-020051-1.50008-5.
[51] V.Y.S. Lee, G. Henderson, A. Reip, T.G. Karayiannis, Flow boiling characteristics in plain and porous coated microchannel heat sinks, Int. J. Heat Mass Transf. 183 (2022) 122152, https://doi.org/10.1016/j.ijheatmasstransfer.2021.122152.
[52] S.J. Darges, V.S. Devahdhanush, I. Mudawar, Assessment and development of flow boiling critical heat flux correlations for partially heated rectangular channels in different gravitational environments, Int. J. Heat Mass Transf. 196 (2022) 123291, https://doi.org/10.1016/j.ijheatmasstransfer.2022.123291.
[53] Y. Katto, H. Ohno, An improved version of the generalized correlation of critical heat flux for the forced convective boiling in uniformly heated vertical tubes, Int. J. Heat Mass Transf. 27 (1984) 1641–1648, https://doi.org/10.1016/0017-9310(84)90276-X.